

# A comparative study of mechanical and microstructural characteristics of aluminium and titanium undergoing ultrasonic assisted compression testing

Haiyang Zhou<sup>a</sup>, Hongzhi Cui<sup>b</sup>, Qing-Hua Qin<sup>a,\*</sup>, Hui Wang<sup>a,c</sup>, Yaogen Shen<sup>d</sup>

<sup>a</sup> Research School of Engineering, Australian National University, Canberra ACT 2601, Australia

<sup>b</sup> College of Civil Engineering, Shenzhen University, Shenzhen 518060, Guangdong, China

<sup>c</sup> Institute of Scientific and Engineering Computation, Henan University of Technology, Zhengzhou 45001, China

<sup>d</sup> Department of Mechanical and Biomedical Engineering, City University of Hong Kong, 83 Tat Chee Avenue, Kowloon Tong, Hong Kong, China

## ARTICLE INFO

### Keywords:

Ultrasonic vibration  
Aluminium  
Titanium  
Residual effect  
EBSD  
Yield point elongation

## ABSTRACT

The mechanism of ultrasonic softening effect has been widely investigated and used in the metal material processing area. Deficiency discussion, however, has been focused on the residual effect of ultrasonic vibration on the plasticity of metals only. In this study, ultrasonic vibration assisted compression (UAC) experiments were carried out using commercially pure aluminium and titanium samples. Despite the similar ultrasonic softening effect, different ultrasonic residual effects were observed in the aluminium and titanium samples. Aluminium exhibited a residual hardening phenomenon, whereas in titanium the initial residual hardening effect transferred to a residual softening effect with an increase in amplitude of the applied ultrasonic vibration. Electron backscatter diffraction (EBSD) characterizations revealed that substructure multiplication, texture evolution and dynamic recrystallization caused by the ultrasonic vibration are the main causes of the residual hardening effect of aluminium. The boundary strengthen mechanism based Hall–Petch relationship was used to explain the mechanism and to predict the influence of the ultrasonic residual effect for aluminium. For the titanium, it was found that the ultrasonic vibration reduced the density of deformation twinning in the specimen, and the evolution of residual effect was analysed from the aspects of grain refinement, deformation twinning induced strain hardening. By quantitative study, the main reason for the residual hardening effect of UAC aluminium sample is identified to be the ultrasonic vibration induced grain refinement, while for the titanium, the weakened strain hardening effect induced by deformation twinning should be the main factor accounting for the residual softening of titanium. Also the ultrasonic vibration could have a similar influence as that of the thermal treatment to the titanium sample, resulting in the yield point elongation (YPE) phenomenon.

## 1. Introduction

The effect of ultrasonic vibration during plastic deformation of metal materials was first reported by Blaha and Langenecker in 1955 [1]. In their research, they found that superimposed ultrasonic vibration led to a declining flow stress during the tension test of single crystal zinc, a phenomenon referred as the ultrasonic softening effect. With regard to the ultrasonic softening effect, some studies [2–6] had investigated the relationship between ultrasonic vibration and flow stress reduction. The references [2–4] suggested that the flow stress reduction during ultrasonic assisted processing of metals was related to the ultrasonic intensity, which is proportional to the square of the vibration amplitude. However, works in references [5,6] indicated that the flow stress reduction was proportional to the ultrasonic vibration

amplitude. Possible mechanisms of the ultrasonic softening effect have been proposed as: i) stress superposition [7–10]; ii) thermal softening [11]; and iii) change of surface friction [12]. However, there are some disagreements among these previous proposed mechanisms of the ultrasonic softening effect. For example, the study [13] found that reduction of mean stress was greater than the oscillatory stress induced by ultrasonic vibration. Moreover, according to the references [13–15], the temperature change caused by superimposed ultrasonic vibration is very limited. Despite these disagreements, the idea is generally accepted that, by superimposing ultrasonic vibration on the deformation process of metals, the forming load is significantly reduced. Based on this concept, some ultrasonic vibration assisted material processing technologies had been developed, such as ultrasonic metal welding or ultrasonic consolidation [16–20], ultrasonic vibration assisted wire

\* Corresponding author.

E-mail address: [qinghua.qin@anu.edu.au](mailto:qinghua.qin@anu.edu.au) (Q.-H. Qin).

drawing [21–23] and ultrasonic shot peening [24,25].

Apart from the ultrasonic softening effect, ultrasonic residual softening and residual hardening effect have also been reported in the literature. Yao et al. [6] found the residual hardening effect during the acoustic vibration assisted aluminium compression test. In their modelling work, the residual hardening effect was attributed to the multiplication of dislocation density. It is noted that a residual softening effect is also possible, as reported in previous studies of Huang et al. [5] and Lum et al. [26], in which the annihilation of dislocation was believed to be the cause inducing this residual softening effect. But the two research groups [5,26] did not conduct direct microstructure analysis to support their construction. Moreover, the effect of ultrasonic vibration on the microstructure evolution was investigated by Siu et al. [15]. During indentation of aluminium it was found that a very pronounced sub-grain formation occurred when horizontal ultrasonic vibration was applied. This observation was interpreted as the enhanced dipole annihilation caused by ultrasonic vibration. On the other hand, in the work of Dutta et al. [27], sub-grain formation was substantially reduced in a carbon steel sample with in situ horizontal ultrasonic treatment. According to the analysis of Dutta et al., this inconsistency could be due to the difference of deformation mechanisms between face-centred cubic (FCC) metal and body-centred cubic (BCC) metal. The evolution of dominant dislocation types during the deformation of BCC metal may also contribute to this difference. Given the fact that the loading conditions were quite different in these two studies mentioned above, sub-grain formation or annihilation mechanisms and their relationship to ultrasonic vibration still need to be investigated for different metals with different crystal structures. It is found that in both the microstructure characterization mentioned above, the effect of microstructure evolution on the mechanical response of materials was not considered.

As was shown in Fig. 1, although ultrasonic vibration has both a softening effect and residual effects during the metal forming process, the residual effects can significantly change the mechanical properties of materials. Previous studies have mainly focused on the ultrasonic softening effect and its applications, whereas for the present study, the lightweight metals aluminium and titanium, which have been widely used in the automotive and aerospace industries [28–31], were chosen as subjects. It is noted that aluminium with FCC crystal structure and titanium with hexagonal close-packed (HCP) structure have different deformation mechanisms. The main objectives of this study are to study the mechanical behaviour of materials after ultrasonic vibration assisted deformation and to investigate the mechanism underlying

changes in mechanical behaviour induced by the microstructural evolution of materials.

## 2. Experimental

### 2.1. Materials and samples

The commercially pure materials: aluminium Al1060 and titanium ERTA1ELI were used for this study. The aluminium Al1060 raw material (supplied by SWA Co., Ltd.) came as annealed aluminium bar manufactured under China technical standard GB/T3880.2-2006, with a diameter of 6 mm, and then was machined along the axial direction of the bar into cylindrical samples with both diameter and height of 4 mm. The commercially pure titanium ERTA1ELI (supplied by BAOTAI Co., Ltd.) came as an annealed titanium bar manufactured under China technical standard NB/T47018.7-2011, with a diameter of 2.4 mm, and then was machined along the axial direction of the bar into cylindrical samples with both diameter and height of 2.4 mm. As the materials were already annealed, no further heat treatment was applied to both aluminium and titanium samples after machining. Also since the machined surface of the sample ends was fine and flat for present study, so no further polish was conducted after machining. The chemical compositions of the materials are given in Table 1.

### 2.2. Ultrasonic assisted compression

An ultrasonic vibration unit was designed to carry out the ultrasonic vibration assisted compression (UAC) experiments with aluminium Al1060 and titanium ERTA1ELI samples. The ultrasonic vibration unit was assembled on the universal testing machines (Hualong-WDW300), as shown in Fig. 2(a). During the UAC process, the crosshead moved upward and the specimen was compressed by the crosshead to the flat compression mould to a certain strain first, then the ultrasonic vibration was directly applied to the specimen through the ultrasonic horn in the vertical direction during compression, no medium was used to couple between the ultrasonic horn and specimen. After a few seconds the vibration would be stopped and the crosshead kept moving until the specimen was compressed to about half of the original height. The schematic of the loading procedure is showed in Fig. 2(b). In the experiment, the vibration frequency applied to the samples was 30.8 kHz. The vibration amplitude was measured by a Doppler Vibrometer (PSV-400) when there was 3000 N load (the maximum load to the sample subjecting to ultrasonic vibration) and no load on the sample, based on the method of [13]. The relationship of the vibration amplitude and the input voltage in different loading conditions is shown in Fig. 3, which indicated that the loading condition had little influence to the vibration amplitude, and the vibration amplitude had a nearly linear relationship with the input voltage to the transducer. In the tests, the loading was controlled by the displacement of the crosshead per minute, which was also considered as the compression speed of the specimens. During the tests, the load train calibration was carried out by conducting the compression test without specimen to eliminate the influence of the elastic deformation of the vibration unit as well as universal testing machine. The crosshead moved up to compress the ultrasonic horn directly to the flat compression mould without sample until the load reached 8000 N, and the displacement of the crosshead was recorded as the elastic deformation of the universal testing machine and the vibration unit. By subtracting this elastic deformation from the recorded displacement of crosshead during UAC test with sample, the achieved result is the deformation of the sample, as shown in Fig. 4. The engineering strain of the specimen was directly calculated based on the calibrated displacement of the crosshead and then transferred to the true strain to evaluate the deformation of the specimens. In this study both aluminium and titanium samples were compressed to half of the original height, so the engineering strain of the aluminium sample was 0.5, the corresponding true strain was

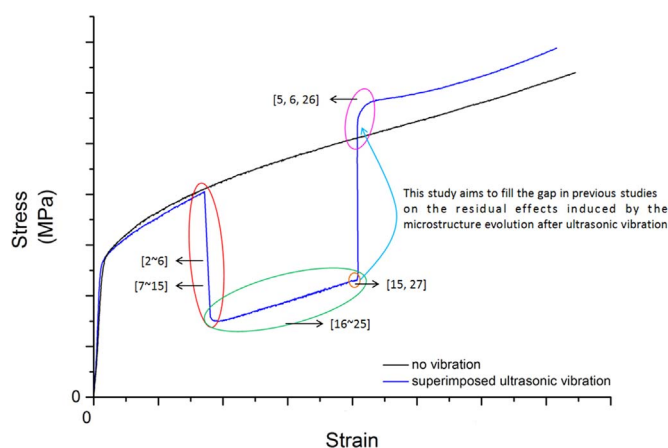


**Fig. 1.** Schematic of the focuses of previous studies and contribution of this study: [2–6] relationship between ultrasonic softening and the ultrasonic vibration amplitude; [7–15] mechanisms of ultrasonic softening; [16–25] application of ultrasonic softening in materials processing; [15,27] microstructure evolution after deformation induced by ultrasonic vibration; [5,6,26] ultrasonic residual effect; this study aims to fill the gap marked on the curves.

**Table 1**  
Chemical composition of commercially pure aluminium Al1060 and titanium ERTA1ELI in wt%.

Al1060 (O3)	Al	Si < 0.25	Cu < 0.05	Mg < 0.05	Zn < 0.05	Mn < 0.05	Ti < 0.03	V < 0.05	Fe 0–0.40
ERTA1ELI(M)	Ti	Fe 0.02	C < 0.01	N < 0.01	H 0.02	O 0.08			

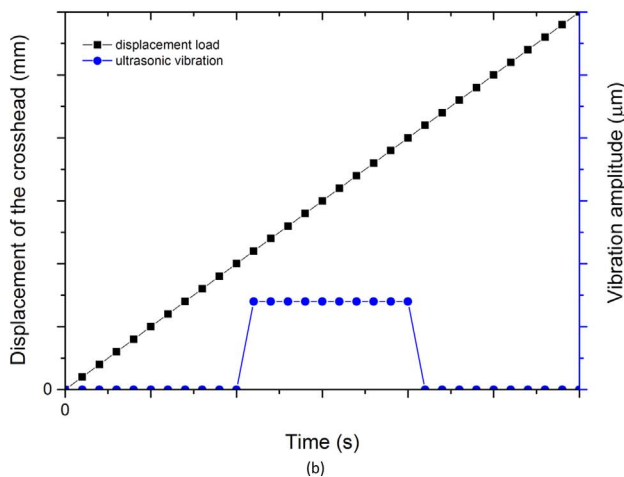
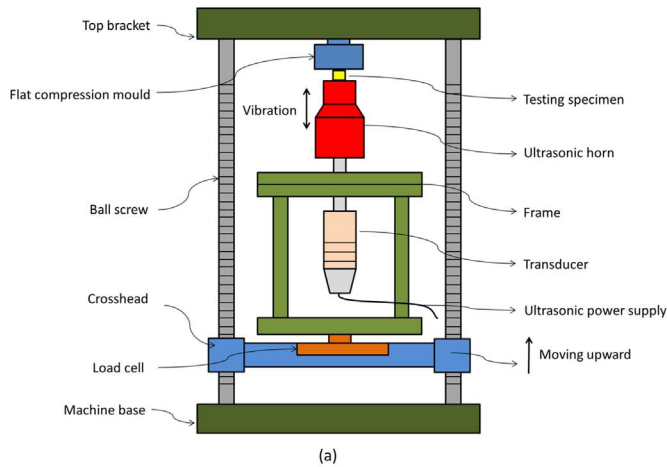


**Fig. 2.** (a) Experimental setup for ultrasonic vibration assisted compressive tests with (b) Schematic of the loading procedure of the UAC process.

about 0.69. To achieve a constant strain rate of  $0.005 \text{ s}^{-1}$ , the compression process should be finished with duration of 138 s, so the speed of cross head for aluminium was about 0.87 mm/min and for titanium it was 0.52 mm/min. To ensure the alignment during the compression, the clearance gauge was used to test if there are gaps between the ultrasonic horn and crosshead during the load train calibration tests, and the ultrasonic frame will be adjusted to make sure that the surfaces of ultrasonic horn and crosshead are parallel to each other. Some detailed experimental methods and parameters are illustrated in the Results section.

### 2.3. Microstructure characterization

Both aluminium and titanium specimens with different strain states and compression processes were prepared for EBSD analysis as shown in Fig. 5. The cylindrical sample was cut in half along the longitudinal axis. All the samples were gradually ground on SiC paper with the grit of 2000#, 3000#, 5000#, and 7000#. Then a 1 µm diamond suspension was used to fine polish the sample. The final mechanical-chemical

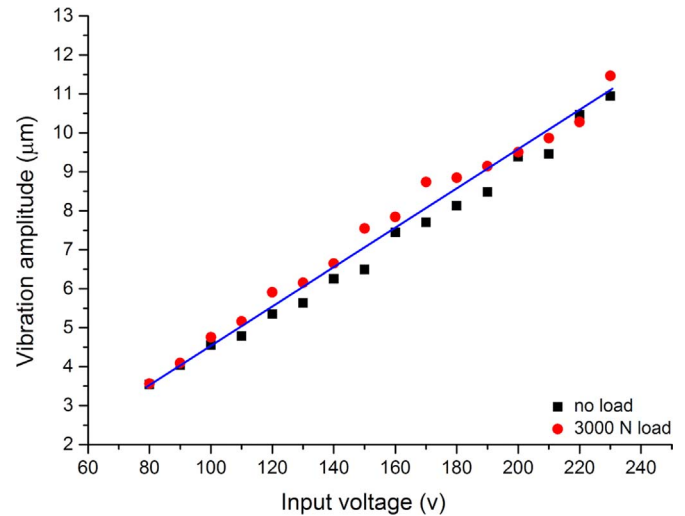


**Fig. 3.** Vibration amplitude of the horn surface at different input voltages under different load conditions.

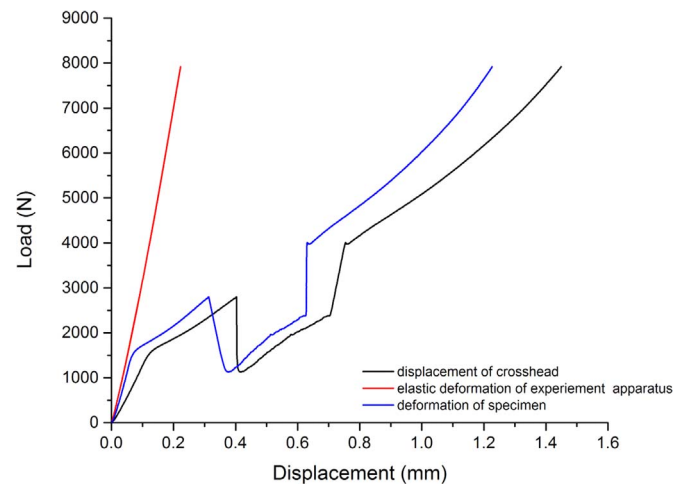


**Fig. 4.** Schematic of the load train calibration and measurement of the specimen deformation.

polishing of aluminium samples was done using 0.02 µm colloidal silica solution and a mixture polishing solution of hydrogen peroxide (30%) and colloidal silica with a ratio of 1: 5 was used for the titanium samples.

EBSD testing was carried out on the Zeiss UltraPlus analytical FESEM at the centre of the samples with the accelerating voltage of 20 kV, beam current of 4 nA and working distance of 24.5 mm. The step size used for all the initial specimen without deformation was 1 µm and a step size of 0.4 µm was used for all the deformed samples to balance the mapping accuracy and efficiency. More details are given in the Results section. The EBSD data was post-processed through HKL Channel 5 system.

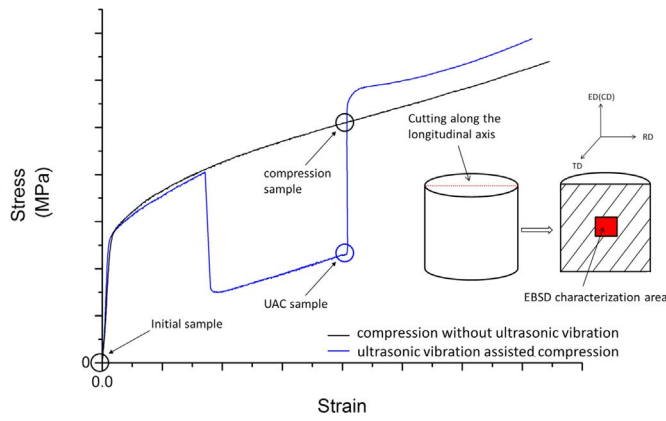


Fig. 5. Schematic of EBSD samples' strain state and compression process.

### 3. Results and analysis

#### 3.1. Softening and residual effects of ultrasonic vibration

A series of UAC tests with different vibration amplitudes and vibration durations were conducted on both aluminium and titanium samples. As shown in Fig. 6(a) and (b), all the aluminium and titanium samples were first compressed to a strain of about 14%, then the ultrasonic vibration with different amplitudes was applied to the samples vertically. The compression process was assisted by the ultrasonic vibration until the samples reached a strain of 32%. Then the ultrasonic vibration was stopped and the compression process

continued until the samples reached a strain of about 75%. For both aluminium and titanium samples the total vibration time was about 36 s.

When the ultrasonic vibration was applied to the samples (to both aluminium and titanium), there was a significant reduction of true stress together with a slightly increased strain. After the stress dropped to its lowest point, it gradually increased with an increase in the deformation. When the ultrasonic vibration was stopped, the stress of the aluminium and titanium samples increased linearly with the strain, indicating an elastic deformation process. Afterwards, during the subsequent compression process, the stress of the aluminium samples which had been ultrasonically vibrated was higher than that under the normal compression, indicating that there was a residual hardening effect in the aluminium samples. In a simple uniaxial compression test, the ratio of the von Mises equivalent stress to the hydrostatic stress is 3 and the hydrostatic stress is a dilatational component. In this study, the UAC is uniaxial compression test, there were not any surrounding constrains for the samples and the samples can be expanded freely, therefore, the effect of the hydrostatic stress on the sample deformation could be neglected.

It is also observed from Fig. 6(b) that, in the titanium samples, there was a transition process of the residual effect: when the vibration amplitude was 4.1  $\mu\text{m}$ , there was a residual hardening effect. However, when a higher vibration amplitude, say 5.6  $\mu\text{m}$ , was applied, there was no noticeable residual effect. When the vibration amplitude was 6.4  $\mu\text{m}$  or above, an obvious residual softening effect was emerged. In the present study for the titanium samples, a yield point was achieved during the subsequent compression process after ultrasonic vibration with the amplitude of 8.5  $\mu\text{m}$  or above was superimposed. With the

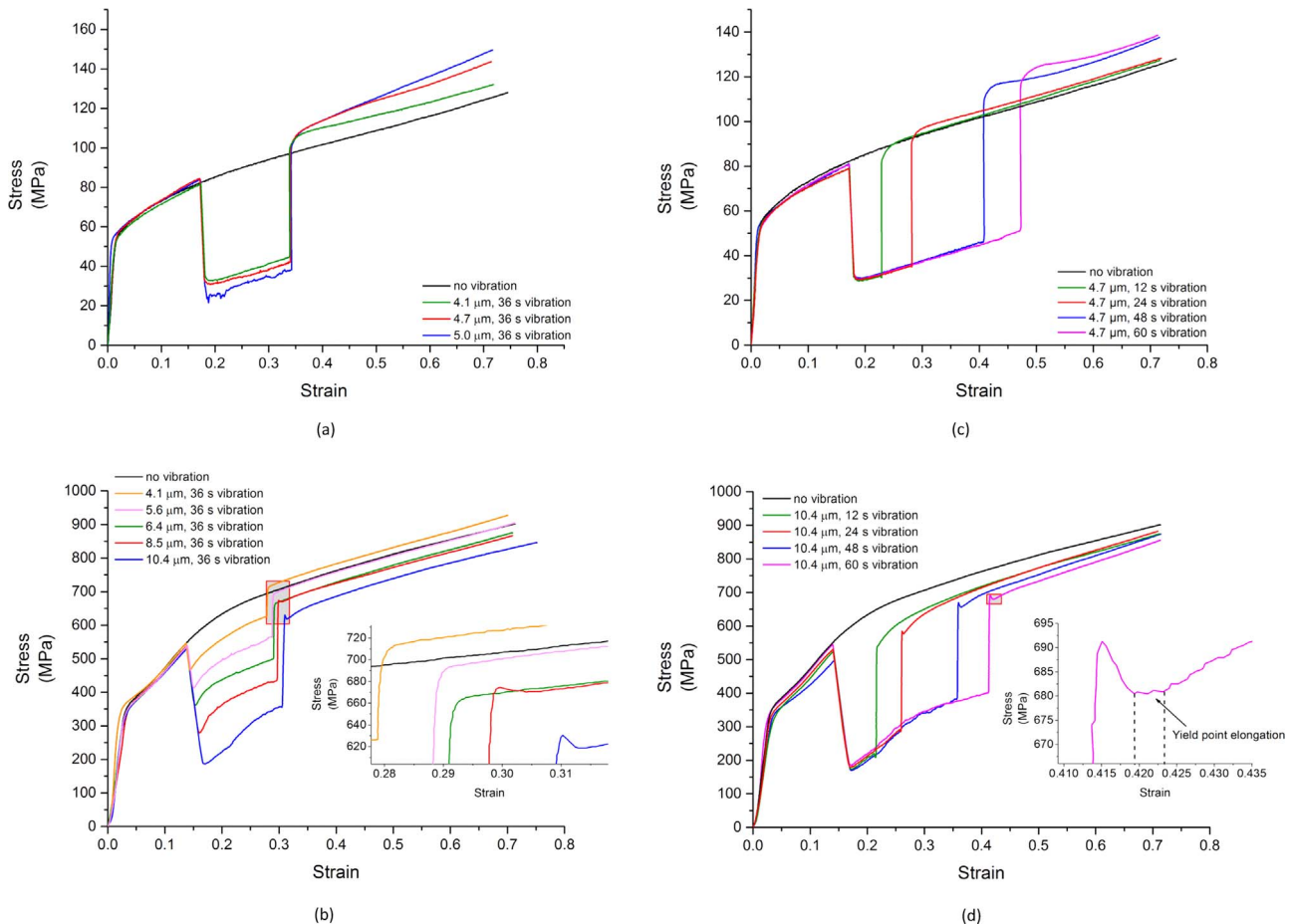


Fig. 6. Softening and residual effects of ultrasonic vibration with different vibration amplitudes on samples of (a) aluminium and (b) titanium. Softening and residual effects of ultrasonic vibration with different vibration durations on samples of (c) aluminium and (d) titanium.

application of higher vibration amplitudes, the ultrasonic softening effect and the ultrasonic residual effects, both the hardening effect for aluminium and the softening effect for titanium, were enhanced. Fig. 6(c) and (d) depict the effect of the duration of ultrasonic vibration on aluminium and titanium samples respectively. In general, the longer the vibration time, comparing with the compression sample, the more residual hardening effect was accumulated for the UAC aluminium samples. Specifically for the titanium samples shown in Fig. 6(d), a short time of ultrasonic vibration provided a residual softening effect. However, there was no obvious yield point during the following compression process. Only when the vibration time was long enough, 24 s or above in particular, did the yield points occur. When the vibration duration was 60 s, a yield point elongation phenomenon with a length of 0.39% strain was observed. The yield stress of titanium was reduced comparing with the true stress of the conventional compression sample experiencing the same strain.

These UAC experiments indicate that ultrasonic vibration can dramatically reduce the true stress of deformation in both aluminium and titanium. During the ultrasonic vibration process, some microstructure evolution in the aluminium and titanium samples must have caused the subsequent residual effects. In the next part, the microstructural analyses of aluminium and titanium through EBSD were used to explain the formation of the residual effects.

### 3.2. EBSD analysis

#### 3.2.1. EBSD characterization of aluminium

EBSD characterization was conducted for aluminium, as mentioned above. The compression sample was prepared with a strain about 46%. The UAC sample was first compressed to a strain of 14%, and then the ultrasonic vibration was applied until the sample reached the strain of 46%, and the total vibration lasted for about 60 s.

Band contrast maps with grain boundaries of aluminium are shown in Fig. 7. It is obvious that the compression (Fig. 7(b)) as well as the UAC (Fig. 7(c)) both introduce low angle (2–15°) grain boundaries to the samples compared with the initial sample (Fig. 7(a)). The greatest number of low angle grain boundaries appear in the UAC vibrated sample and many of the low angle grain boundaries have a closed shape within the large grains with high angle grain boundaries, indicating that the compression increases the number of substructures, such as sub-grain boundaries in the aluminium and that, with the application of ultrasonic vibration, the formation of sub-grain is promoted. The substructures induced by deformation result in grain size evolution in the samples and, along with the grain size evolution, there is also a change of grain geometry during the deformation. In Fig. 7(b) and (c), the grains after compression and UAC have an elongated geometry compared to the original relatively equiaxed grains. By the line intercept method (30 lines per graph), the average distances between boundaries with different angles were calculated along both the compression ( $d_{CD}$ ) and transverse directions ( $d_{TD}$ ) from Fig. 7. The statistical values are listed in Table 2.

The commercially pure aluminium bar was rolled along the longitudinal axis, which was also the compression direction in this study, so the distance between the boundaries along the compression direction was greater than that along the transverse direction. The result was evidenced by the fact that the  $d_{CD}/d_{TD}$  ratios for all three cut-off angles were nearly the same (the  $d_{CD}/d_{TD}$  ratio ranging from 1.11 to 1.20). In the compressed and UAC samples, the diameters along both the compression and transverse directions were small, due to the encasement of sub-grain boundaries induced by the deformation. Compared with the compression sample, the UAC sample had an even smaller grain size. And for the compression sample, the  $d_{CD}/d_{TD}$  ratio was around 0.65. It varied only a little for all three cut-off angles. For the UAC samples, however, the  $d_{CD}/d_{TD}$  ratio for grain boundaries above 2° was higher than those for both 10° and 15°. In addition, the ratio was also higher than those from the corresponding data of compressed

samples. Since the sample size and the strain state of the compression and UAC specimens are the same, a higher  $d_{CD}/d_{TD}$  ratio for the UAC sample implies that the induced sub-grain boundaries by the ultrasonic vibration were more tend to be perpendicular to the compression direction.

During the deformation process, the texture of the aluminium was changed. The distributions of misorientation angle, both correlated (misorientation data between neighbouring points) and uncorrelated (misorientation data between randomly chosen points), in the three aluminium samples are shown in Fig. 8. For the initial materials, the misorientation angles are relatively evenly spread, while for the compression and UAC sample most of the correlated misorientation angles are below 15°. And in the initial material, the correlated and uncorrelated misorientation angles almost have the same distribution, indicating that the misorientation angles are relatively randomly distributed which is caused by the annealing process. For the compression sample, the correlated misorientation angles ranges from 2° to 36°. These angles are mainly concentrated in the range of 2° to 15°. However, for the uncorrelated misorientation angles, though they are distributed in the same range with the correlated ones, the distribution is more tend to be a normal distribution. This distribution is caused by the compression induced reorientation of grains. Due to the compression a strong texture was achieved in the sample. For the UAC sample, the correlated misorientation angle distribution has a similar trend with the one in the compression sample; most of the misorientation angles range from 2° to 15°. But there is also a number of misorientation angles ranging from 15° to 60°, whereas in the compression sample, the highest misorientation angle is only about 36°. As for the uncorrelated misorientation angles, their distribution in UAC are quite evenly by comparison to the normal distribution in compression sample. The distribution of uncorrelated misorientation in UAC sample ranges from 2° to about 61°. This indicates that the ultrasonic vibration caused crystallite rotation during the compression process. Thus, a small amount of high angle grain boundaries formed. The grain rotation will cause the texture evolution in the UAC sample.

The orientation distribution functions (ODF) of three aluminium samples are shown in Fig. 9. In the initial material there is a strong fibre texture  $\langle 100 \rangle || ED$  (CD) and the maximum pole density is 35.5. Then, after compression, the initial fibre texture was removed by the deformation and a strong Goss texture  $\{110\} \langle 001 \rangle$  with the maximum pole density of 73.3 was achieved. For the UAC sample, it shows a similar Goss texture as the compression sample, but the maximum pole density is only 22.8. And some concentrations of the Euler angles can also be observed near the Goss texture, as shown in Fig. 9(c) with  $\varphi_2$  being equal to 20°, 60° and 65°, respectively. These concentrations were not presented in the ODF of compression sample. So it is confirmed that the ultrasonic vibration caused crystallite rotation and weakened the Goss texture shown in the compression sample.

The recrystallization grain fraction obtained from EBSD data is shown in Fig. 10. When the initial material was annealed, it had a large fraction of recrystallization grains (about 80%) 15.9% grains were substructured, and 4.1% grains were deformed as shown in Fig. 10(a). After compression, 59.4% of grains were substructured, 33.4% of grains were deformed and only 7.2% of the grains were recrystallized. After UAC was applied, most of the grains are deformed with a fraction of 73.2% and 20.8% of the grains are substructured, as for the recrystallized grains, they only take a fraction of 6%. For the compression sample, the majority of the grains are substructured. With the applied ultrasonic vibration, the average misorientation angles within the grains were increased, resulting in a large fraction of deformed grains. This also indicated that the ultrasonic vibration induced the crystallite rotation within the grains during the UAC process and it was evidenced by the fact that the density of Goss texture was weakened in the UAC sample comparing with the compression sample as mentioned above. With a larger and evenly distributed deformed grains, it is obvious that the ultrasonic vibration can promote the sample to be

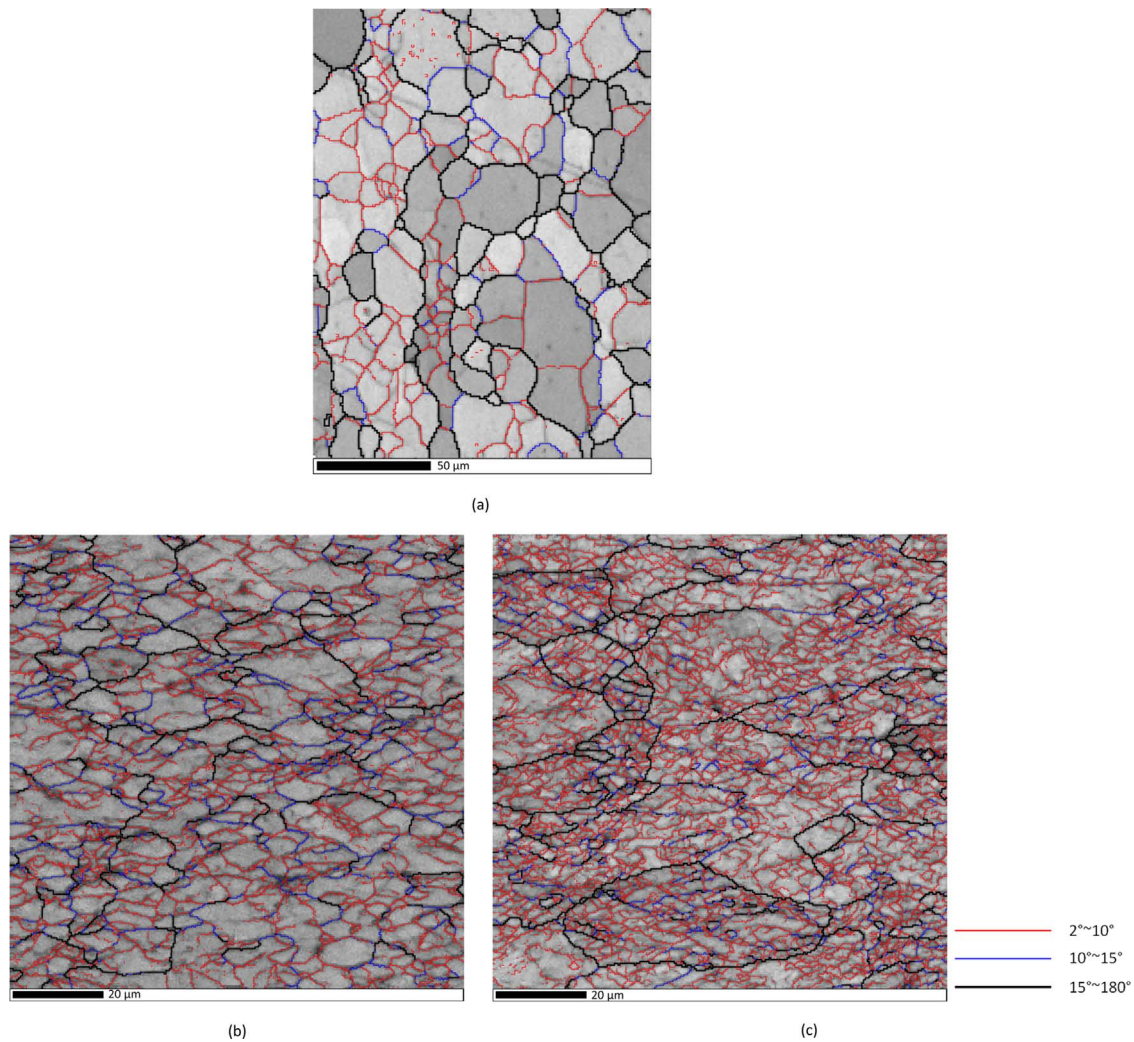


Fig. 7. Band contrast map with grain boundaries of (a) initial material, (b) compression sample, and (c) UAC sample.

**Table 2**

Average distance between boundaries along compression and transverse directions..

Condition	Angle (deg)	$d_{CD}$ ( $\mu\text{m}$ )	$d_{TD}$ ( $\mu\text{m}$ )	$d_{CD}/d_{TD}$ ratio
Initial	2	10.95	9.12	1.20
	10	17.33	15.62	1.11
	15	22.40	20.06	1.12
Compression	2	2.14	3.31	0.65
	10	5.56	9.14	0.61
	15	10.70	15.63	0.68
UAC	2	1.55	2.17	0.71
	10	5.10	8.86	0.58
	15	8.56	13.98	0.61

deformed more homogeneously. Comparing the UAC sample with the compression one, the fraction of recrystallized grains does not change much. It is noticed that, by giving different definitions of the range of misorientation angles within the recrystallized, deformed and substructured grains, different fractions of these three kinds of grains can be obtained. In this study, though fractions of recrystallization grains of three samples were given, the objective was to qualitatively illustrate the effect of ultrasonic vibration to the dynamic recrystallization of aluminium.

To investigate the effect of textural evolution on the mechanical performance of aluminium, the Taylor factors of all three aluminium samples along the compression direction were calculated from the EBSD data. The Taylor factor has a trend to increase with deformation.

When the ultrasonic vibration was applied the average Taylor factor was the highest, as shown in Fig. 11. The average Taylor factors for the initial, compressed and UAC materials are 2.438, 2.410 and 2.681 respectively.

### 3.2.2. EBSD characterization of titanium

EBSD characterization was carried out on the UAC titanium sample with a strain about 50%. The specimen was first compressed to a strain of 14%, and then the ultrasonic vibration was applied to the specimen and lasted for 72 s.

Different from the FCC aluminium,  $\alpha$  phase titanium sample used in this study has a HCP crystal structure, with a  $c/a$  ratio of 1.587 which is below the ideal ratio of 1.633. And the easy  $\langle 1120 \rangle$  slip direction is perpendicular to the  $c$ -axis, so the slip on the easy planes cannot produce any deformation along the  $c$ -axis. To accommodate the strain in the  $c$ -direction, the slip system as well as the twinning system with a direction of  $\langle c+a \rangle$  would be operative. Fig. 12 shows the band contrast map with high angle grain boundaries and twinning boundaries of titanium.

In the well annealed initial material, most of the grains are equiaxed, and there are no twinning boundaries in the initial material. After being compressed to a strain of 50%, there are lots of twins with misorientation angles of  $64^\circ$  and  $85^\circ$  occurred in the specimen, as shown in the Fig. 12(b). It is noted that grains size are not as even as the initial ones. A numerous small grains were produced with surrounding large grains. For the UAC specimen, as shown in

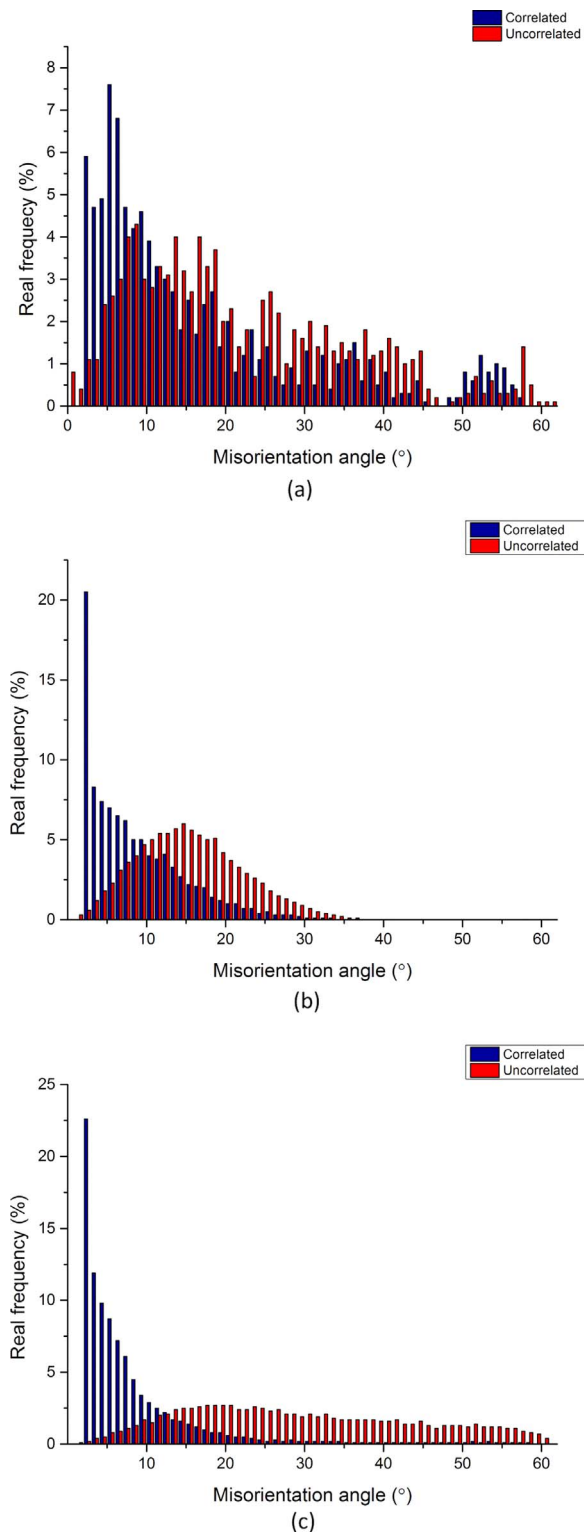


**Fig. 8.** Misorientation angle distributions of (a) initial material, (b) compression sample, and (c) UAC sample of aluminium.

Fig. 12(c), the grain size distribution is similar to the compression sample. However, there are only a few twinning boundaries which can be detected from the UAC sample. And the grain boundary map shows a clear plastic flow perpendicular to the compression direction. The average distance between boundaries with different cut off angles and direction is shown in Table 3.

It is found that, comparing with the initial material, both the compression and UAC process can refine the grain size. However, the

grain sizes for the UAC and compression specimen with different cut off angles are quite similar to each other. Thus by comparing with normal compression, the UAC process is less efficient for reducing the grain size for the titanium sample as it did for the aluminium one.

As mentioned above, twinning is another deformation mechanism for the titanium other than the dislocation and slip. There are two kinds of deformation twinning shown in the deformed sample:  $\{10\bar{1}2\} < 10\bar{1}1 >$  tensile twinning and  $\{11\bar{2}2\} < 11\bar{2}3 >$  compressive twinning. The fractions of the length of the different twinning boundaries to the high angle grain boundaries are shown in Table 4. It is found from Table 4 that the total twinning boundaries in the compression sample are 4.7 times to the ones in the UAC sample.

The distributions of misorientation angles for three titanium samples are showed in Fig. 13. As the initial sample was annealed, the correlated and uncorrelated misorientation angle distributions show a similar behaviour with low concentration on the low angle grain boundaries below  $15^\circ$  as shown in Fig. 13(a). For the compression and UAC samples, most of the misorientation angles are distributed in the range of  $2\text{--}15^\circ$ , indicating that large number of low angle grain boundaries were induced by the deformation. And the appearance of deformation twinning is proved by the two peak values occurring in the correlated misorientation angles as shown in Fig. 13(b).

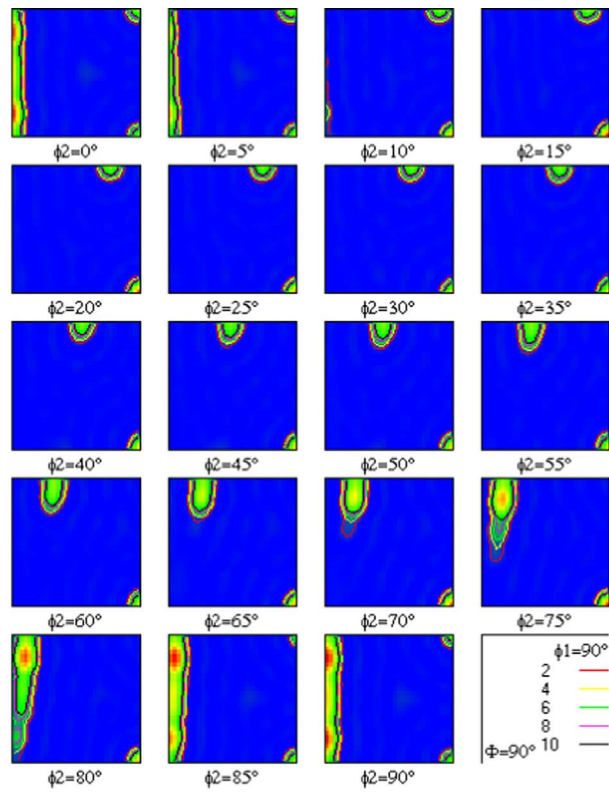
## 4. Discussion

### 4.1. Residual hardening of aluminium

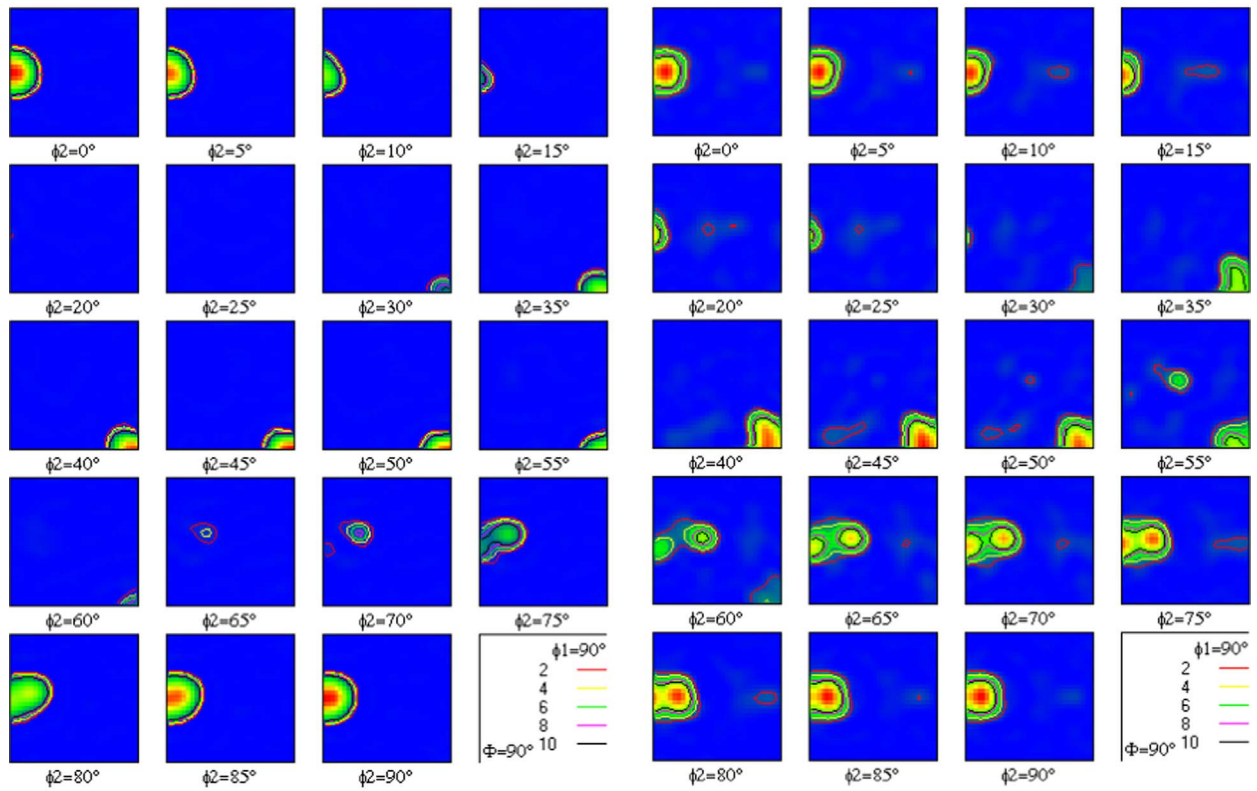
#### 4.1.1. Microstructure evolution in aluminium due to ultrasonic vibration

During the compression deformation of aluminium, the initial grains were compressed and elongated. Within the initial grains, sub-grains of almost equal size generated and appeared more elongated than the initial grains by compression [32]. In this study the UAC promoted the formation of sub-grains. Some studies have revealed the microstructure formation caused by ultrasonic vibration, such as in research into ultrasonic impact treatment (UIT), due to the high dislocation density induced by ultrasonic vibration, more dislocations tended to tangle and rearrange to form sub-grains and, with the mutual rotation of neighbouring sub-grains, nano-scale grain structures being obtained [33–35]. With the application of ultrasonic vibration during plastic deformation, an oscillatory stress field is superimposed onto the initial driving stress field. According to reference [15], this superimposed stress field leads to the formation of sub-grains via enhancing dipole annihilation. In the present study, with a critical misorientation angle of  $2^\circ$ , the average distance between grain boundaries along the compression direction, as shown in Table 2, decreases significantly from 10.95 to  $2.14\ \mu\text{m}$  due to the compression-induced substructures. Normally during plastic deformation, substructure or grain size reduces with increasing strain until a certain large strain is reached, at which there is a balance of dislocation propagation and annihilation. It becomes difficult to form new dislocation walls and dislocation tangles, resulting in difficulty in achieving further substructure refinement. With ultrasonic vibration,  $d_{\text{CD}}$  decreases to  $1.55\ \mu\text{m}$ . This is because the impact induces a high strain rate deformation in the local area, causing a high dislocation density which continues the substructure refinement.

By comparing the  $d_{\text{CD}}/d_{\text{TD}}$  ratio, it was found that for the UAC sample, the  $d_{\text{CD}}/d_{\text{TD}}$  ratio for  $2^\circ$  is higher than the one for  $10^\circ$  and  $15^\circ$ , while for the compression sample the ratios are nearly the same. Considering that the ultrasonic energy is mostly absorbed by the dislocation and other grain defects such as grain boundaries, rather than the whole material [3], thus it can be assumed that ultrasonic vibration has more effects on the low angle grain boundaries, especially sub-grain boundaries. The ultrasonic energy absorbed by the grain boundaries leads to a more homogeneous deformation. Moreover, UAC



(a)



(b)

(c)

Fig. 9. Orientation distribution functions of (a) initial sample, (b) compression sample, and (c) UAC sample.

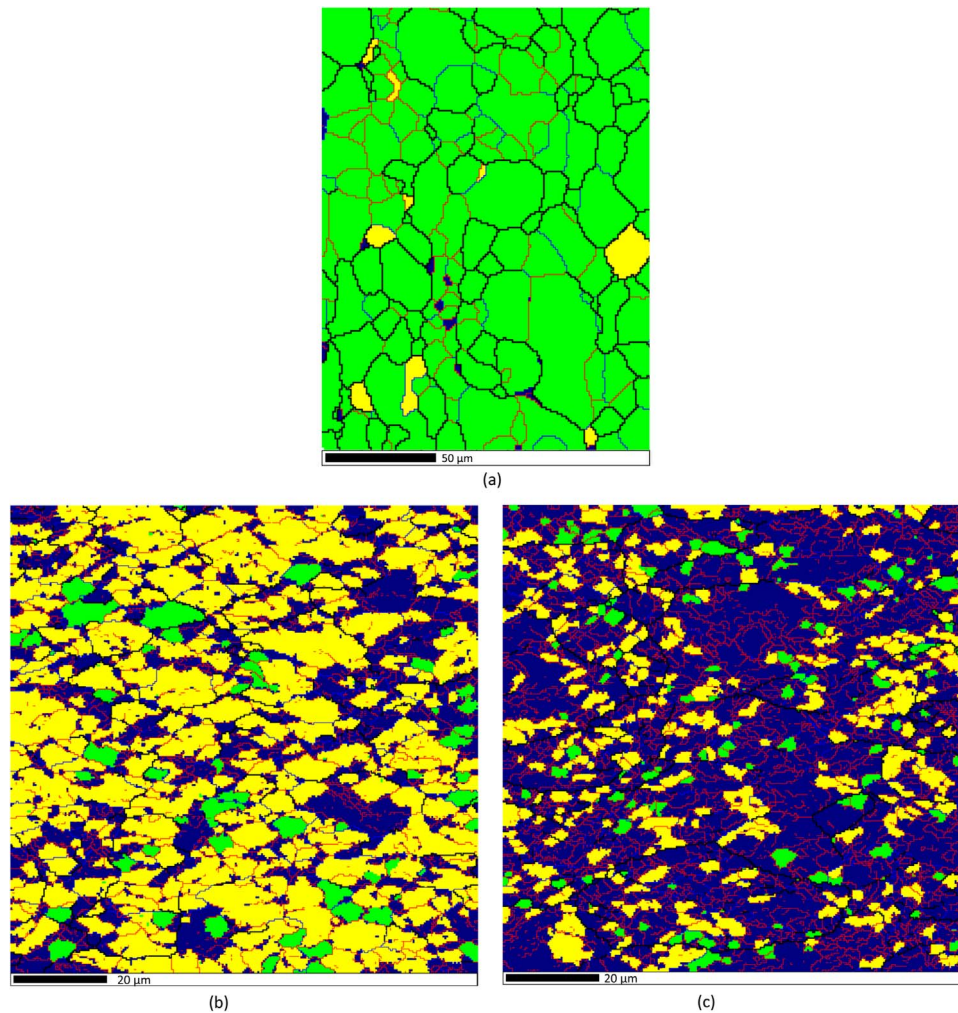


**Fig. 10.** Recrystallized grain fractions of (a) initial material, (b) quasi-static compression sample, and (c) UAC sample. Lime grains represent recrystallized grains with internal average misorientation angle below 1°; Yellow grains represent substructured grains which contains sub-grains, the internal average misorientation angle of the sub-grain is below 1° and the misorientation angle between sub-grains is above 7.5°; and Navy blue grains are deformed grains with internal misorientation greater than 7.5°. (For interpretation of the references to color in this figure legend, the reader is referred to the web version of this article).

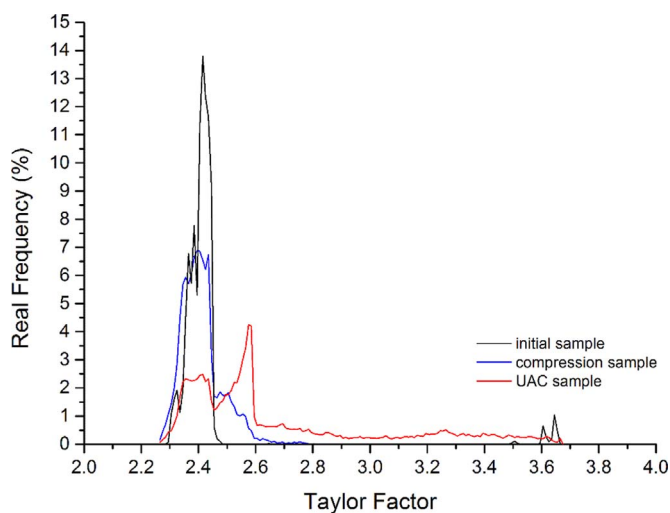


**Fig. 11.** Evolution of Taylor factors with deformation.

has been found to cause grain rotation during tensile testing of low carbon steel [31]. Thus, grain boundary rotation is believed to contribute to the rotational dynamic recrystallization. In this study, the difference in texture between the compressed and UAC samples as

shown in Fig. 9(b) and (c) could be caused by the rotation of grain boundaries, which may lead to the dynamic recrystallization.

#### 4.1.2. Boundary strengthening based on Hall-Petch Model

On the basis of the discussion above, with the application of ultrasonic vibration to the compression test of aluminium, substructures such as low angle grain boundaries (< 15°) and sub-grains will increase and the texture will also evolve, resulting in a change in the Taylor factor in comparison with the compression sample. The microstructural evolution of aluminium will lead to the residual hardening effect. The mechanisms can be explained by the Hall-Petch model and dislocation strengthening. The original Hall-Petch equation shows the relationship between the yield stress  $\sigma_y$  and the grain size as follows [36,37]:

$$\sigma_y = \sigma_0 + k_1 D_{GB}^{-1/2} \tag{1}$$

where  $\sigma_0$  is the flow stress of an undeformed single crystal with orientation for multiple slips. In this study  $\sigma_0$  is taken as 30 MPa [38],  $K_1$  is a constant and  $D_{GB}$  is the grain size.

The relation between flow stress at a certain strain  $\sigma_0(\epsilon)$  and grain size is expressed by the Eq. [39]

$$\sigma(\epsilon) = \sigma_0(\epsilon) + k_1(\epsilon) D_{GB}^{-1/2} \tag{2}$$

In Eq. (2),  $\sigma_0(\epsilon)$  is the flow stress of the grain interior and  $k_1(\epsilon)$

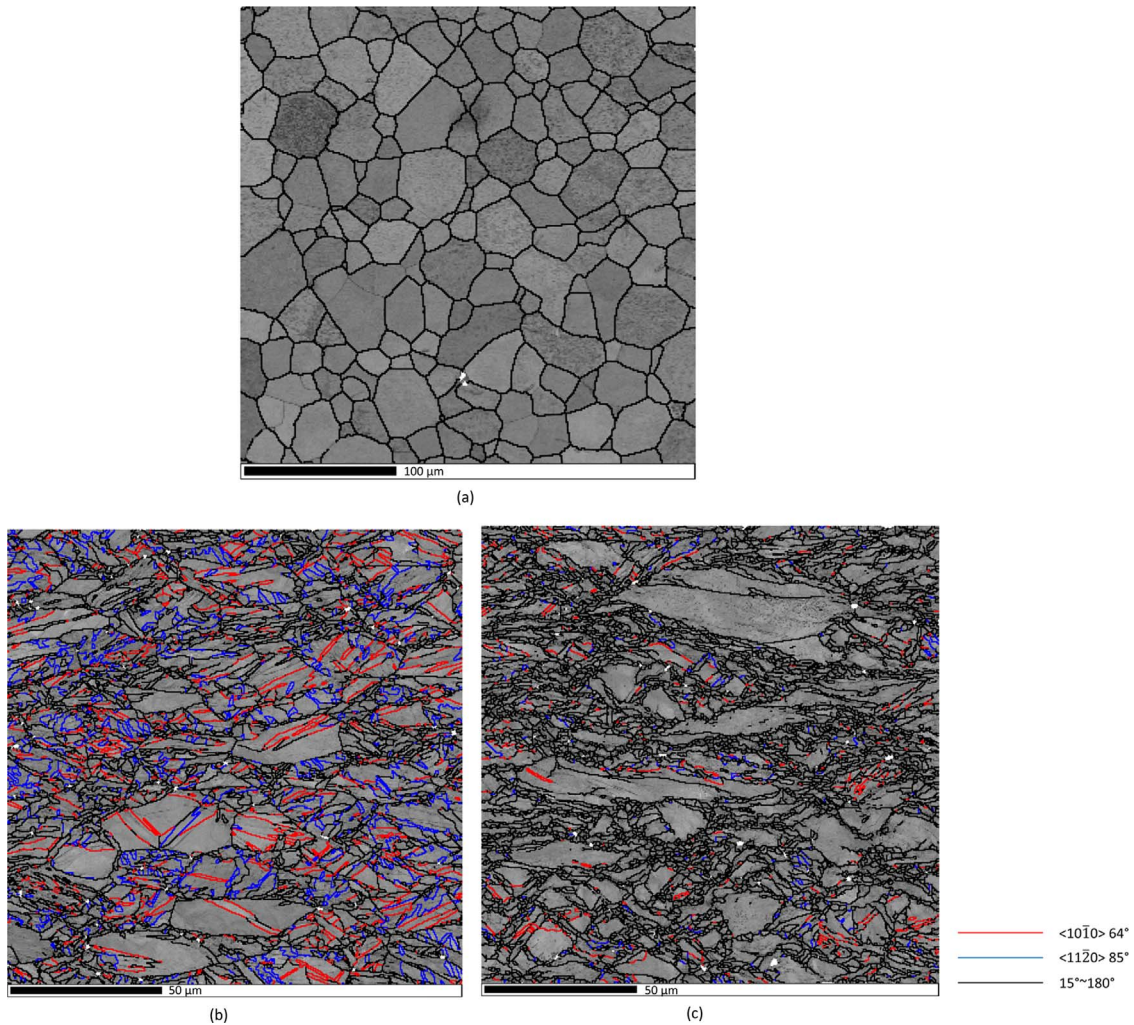


Fig. 12. Band contrast map with twinning boundaries of (a) initial sample, (b) compression sample, and (c) UAC sample.

Table 3

Average distance between boundaries along compression and transverse directions.

Condition	Angle (deg)	$d_{CD}$ ( $\mu\text{m}$ )	$d_{TD}$ ( $\mu\text{m}$ )	$d_{CD}/d_{TD}$ ratio
Initial	2	18.43	18.66	0.98
	10	19.27	19.17	1.01
	15	19.93	19.53	1.02
Compression	2	0.72	0.85	0.85
	10	1.68	2.47	0.68
	15	1.81	2.71	0.67
UAC	2	0.69	0.74	0.93
	10	1.61	2.33	0.69
	15	1.85	2.80	0.66

Table 4

Length fraction of twinning boundaries to the high angle grain boundaries.

Condition	Deformation twinning	Misorientation axis/ Angle	Fraction (%)
Compression	$\{10\bar{1}2\} < 10\bar{1}1 >$	$< 11\bar{2}0 > 85^\circ$	16.82
	$\{11\bar{2}2\} < 11\bar{2}3 >$	$< 10\bar{1}0 > 64^\circ$	17.96
UAC	$\{10\bar{1}2\} < 10\bar{1}1 >$	$< 11\bar{2}0 > 85^\circ$	2.58
	$\{11\bar{2}2\} < 11\bar{2}3 >$	$< 10\bar{1}0 > 64^\circ$	4.86

$D_{GB}^{-1/2}$  represents the strengthening contribution due to the barrier effect exerted by the grain boundaries to the motion of dislocation. In references [40,41], the lamellar structures of deformed metals were

analysed by a combination of extended geometrically necessary boundaries (GNBs) and interconnecting incidental dislocation boundaries (IDBs). The dislocations were assumed to accumulate in the structures' boundaries, and randomly distributed dislocations strengthened the material. The dislocation density in the IDBs could be approximated as  $1.5S_V^{IDB} \cdot \theta^{IDB}/b$ , where  $S_V^{IDB}$  and  $\theta^{IDB}$  are the area per unit volume of IDBs and the average misorientation angle of IDBs,  $b$  is the Burgers vector. Therefore, the flow stress  $\sigma_f$  can be expressed as [42]:

$$\sigma_f = \sigma_0 + M\alpha Gb \sqrt{1.5S_V^{IDB} \cdot \theta^{IDB}/b} + \rho_0 + K_{HP} / \sqrt{D_{av}^{GNB(i)}} \quad (3)$$

where  $M$  is the Taylor factor,  $\alpha$  is a constant taken as 0.24 for aluminium [42],  $G$  is the shear modulus (26 GPa),  $b$  is the Burgers vector (0.286 nm). As the dislocation density between the boundaries  $\rho_0$  is relatively small compared to the dislocation density concentrated on the grain boundaries, it can be neglected [43].  $K_{HP}$  is the slope of the Hall–Petch plot and can be determined by the tensile test of a fully recrystallized polycrystalline sample. For aluminium, the  $K_{HP}$  value can be taken as  $0.04 \text{ MPam}^{1/2}$  [44].  $D_{av}^{GNB(i)}$  is the average slip distance that is related to the perpendicular spacing between GNBs. In the following discussion, the random distance between all boundaries  $D_B$  is used as a substitute for  $D_{av}^{GNB(i)}$  [42].

For grain structures other than lamellar structures such as equiaxed grains, the boundaries are more easily characterized as low angle grain boundaries (LABs) and high angle grain boundaries (HABs) through EBSD, neglecting  $\rho_0$ . Thus Eq. (3) can be rewritten as

$$\sigma_f = \sigma_0 + M\alpha Gb \sqrt{1.5S_V^{LAB} \cdot \theta^{LAB}/b} + K_{HP} / \sqrt{D_B} \quad (4)$$

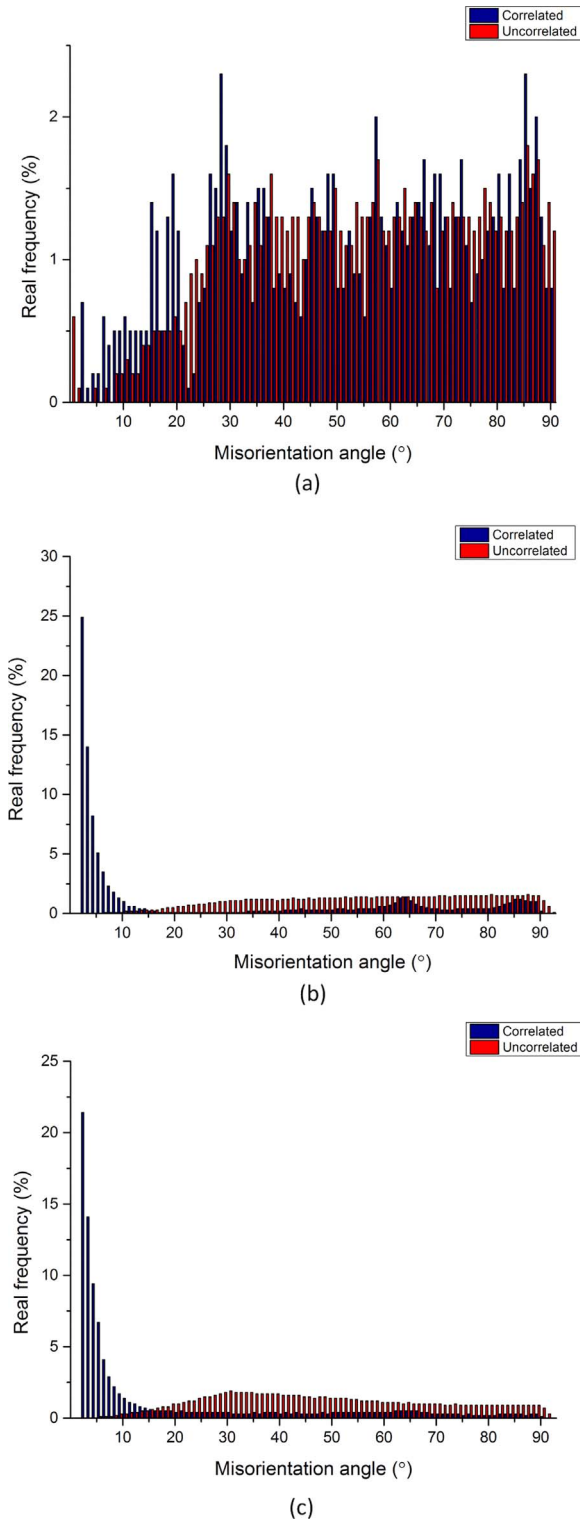


Fig. 13. Misorientation angle distributions of (a) initial material, (b) compression sample, and (c) UAC sample of titanium.

where  $S_V^{LAB}$  and  $\theta^{LAB}$  are the area per unit volume and the average misorientation angle of LABs, respectively. Denoting  $S_V$  as the area per unit volume of all boundaries and the fraction of HABs as  $f^{HAB}$ , the  $S_V^{LAB}$  can be substituted as follows:

$$S_V^{LAB} = S_V(1 - f^{HAB}) \tag{5}$$

Since  $S_V$  equals  $2/D_B$  [45], Eq. (4) can be rewritten as:

Table 5

Parameters for Eq. (6) with different samples.

Condition	$M$	$\theta^{LAB}$	$f^{HAB}$	$D_B$ ( $\mu\text{m}$ )
Initial	2.438	4.745	0.401	10.95
Compressed	2.410	3.313	0.147	2.14
UAC	2.681	3.485	0.138	1.55

$$\sigma_f = \sigma_0 + [M\alpha G \sqrt{3\theta^{LAB}b(1-f^{HAB})} + K_{HP}]D_B^{-0.5} \tag{6}$$

The parameters in Eq. (6) for the initial, compressed and UAC samples were determined by the EBSD data, and are shown in Table 5. The value of  $\theta^{LAB}$  was transformed from degrees to radians for the calculation in Eq. (6).

The calculated true stress for the compressed sample is 107.5 MPa. The value of the calculated yield stress of the UAC sample is 132.2 MPa. For the compression sample, the calculated true stress precisely matches with the experimental data as shown in Fig. 6(c) (no vibration), which is about 106.9 MPa. But by comparing the calculated yield stress of the UAC sample with the  $\sigma_{0.2\%}$  represented offset yield stress of the following compression process after the vibration was stopped showed in Fig. 6(c) (60 s vibration), which is 120.0 MPa; it is found that the calculated yield stress is 10.2% higher than the experimental result. So the boundary strengthening method can give an estimation of the residual hardening effect of aluminium subjected to the UAC process.

#### 4.2. Residual softening of UAC titanium

##### 4.2.1. Evolution of deformation twinning

The deformation twinning is quite sensitive to the deformation rate. Under the high strain rate deformation, the twinning mechanism is more easily triggered [46]. Ultrasonic treatment can normally provide only a small strain change to the material because of the limited vibration amplitude. Due to the high frequency of ultrasonic treatment, however, a high strain rate can still be achieved even with a minor strain change during one cycle of ultrasonic treatment. In this study, when the ultrasonic vibration was applied, the titanium sample was already in plastic deformation status. Under this condition, the ultrasonic vibration is assumed to cause a localized plastic deformation to the sample which can be roughly evaluated by the vibration amplitude, and if this ultrasonic vibration induced plastic deformation was evenly distributed in the whole sample and the deformation is equivalent to the vibration amplitude, the ultrasonic vibration induced strain rate will be about  $640.6 \text{ s}^{-1}$  when a 30.8 kHz vibration with an amplitude of  $10.4 \mu\text{m}$  was applied to the sample. With a localized deformation, the actual strain rate induced by ultrasonic vibration could be even higher. Thus the high strain rate deformation provided by the ultrasonic vibration can promote the development of twinning. Some previous studies of ultrasonic involvement in the processing of titanium, such as in UIT [47,48] and surface mechanical attrition treatment (SMAT) [49], have confirmed the formation of deformation twinning due to ultrasonic treatment. But with the multiplication of the twinning, the number of the twinning will reach to saturation in the deformed specimen, then the twinning will subdivide the grains and each other, leads to the grain refinement as well as the reduce of the twinning boundaries [50]. The high strain rate deformation can accelerate the formation of the twinning, so with the ultrasonic vibration, the saturation point of the twinning will be achieved at a smaller strain comparing with the normal compression. After the saturation of twinning, the number of twinning will drop with continuing deformation and the dominant deformation mechanism for the titanium will be dislocation and slip. So that is the reason why the UAC sample contains only a little twinning comparing with the compression sample, and an obvious trend of plastic flow occurs.

#### 4.2.2. Deformation twinning induced hardening and softening

From the discussion above, deformation twinning is one of the mechanisms of grain refinement because it can subdivide large grains into smaller grains. According to a series of studies by Salem and his colleagues [51–53], during the process of large deformation, large amounts of deformation twinning were induced and caused a strain hardening effect. And the overall strain hardening effect caused by deformation twinning is a combined result of strain hardening via the Hall-Petch mechanism (strengthen by grain refinement caused by deformation twinning), the Basinski mechanism (increase of hardness in the twinned region), and the texture softening due to reorientation of the twinning [53]. Some researchers have investigated the softening effect of deformation twinning. Jiang et al [54] studied the softening effect of deformation twinning of AM30 magnesium alloy, suggesting that although generally the twin boundaries can act as barriers to dislocation motion, they can transform glissile dislocation into sessile dislocation within the twin interior and hence contribute to strengthening via the Basinski mechanism. However, twinning can also accommodate strain along the c-axis to reduce the work hardening effect, and the lattice rotation may also introduce a softening texture to the material. The softening effect of twinning does not occur until the volume fraction of twinning reaches a certain level, which is highly temperature and strain rate related. And HCP titanium will present an overall strain hardening effect due to the deformation twinning during room temperature deformation [53].

In the present study, it is found that the fraction of twinning boundaries in the UAC sample is quite small, only 7.44% in total to the high angle grain boundaries, while in the compression sample this number is 34.78% and the grain size of the UAC sample is similar to the compression one. So with more fraction of deformation twinning, the twinning induced strain hardening effect in normal compression sample is more severe than the UAC sample, and makes the UAC sample with less twinning exhibit a residual softening phenomenon. Also as shown in Fig. 6(b), the residual effect of ultrasonic vibration to the titanium samples gradually transferred from a hardening effect to a softening effect with the increasing vibration amplitude, this change of residual effects can be interpreted from the aspect of evolution of twinning induced by ultrasonic vibration. With low vibration amplitude, the ultrasonic vibration could induce more twinning in the UAC sample than the compression, and cause a residual hardening effect; however with larger vibration amplitude, as discussed, the ultrasonic vibration can cause the saturation of twinning in the UAC sample, and with less twinning in the UAC sample, it will present a residual softening effect comparing with the compression one.

#### 4.2.3. Ultrasonic vibration induced yield point elongation

Normally the HCP titanium exhibits gradual yielding during deformation. However in the present study of yield point elongation (YPE) of HCP titanium conducted by Z Li et al. [55], it is found that after being annealed for 20 min at 500 °C, the grain size of the titanium sample increased from 80 nm to about 0.88 μm and then a yield point elongation phenomenon was observed during the tensile test of the sample. Although in present study all the experiments were carried out in the room temperature, the sample was subjected to the ultrasonic vibration before the occurrence of the residual softening effect and yield point, and the ultrasonic vibration caused unload effect to the sample as well as provided additional energy input to the sample. The energy input through ultrasonic vibration is similar to the thermal input but only more effective as it can directly act on the defects of the material rather than the whole sample [3]. And as shown in Fig. 6(d), after 60 s ultrasonic vibration treatment, there was YPE phenomenon observed during the compression process of the titanium sample. So the ultrasonic vibration could just played the same role as the thermal treatment in the work of [55] and resulted the appearance of yield point of titanium. According to the [55], the dislocation behaviour and grain size influence are the main reason for YPE of titanium rather than

the effect of twinning as reported in study of the YPE phenomenon magnesium in [56]. The ultrasonic vibration induced yield point of titanium is positively related to the vibration amplitude and duration, and comparing with the gradual yielding, the occurrence of yield point could also contribute to the residual softening effect on titanium.

## 5. Conclusion

UAC tests of aluminium and titanium were performed in this study. The stress and strain relation in UAC testing of both aluminium and titanium showed a similar ultrasonic softening effect, but the residual effects of ultrasonic vibration on aluminium and titanium were different. In aluminium, based on the EBSD analysis, the ultrasonic vibration was found to cause the grain refinement and crystallite rotation, such that the residual hardening effect could be explained by the boundary strengthen mechanism based Hall-Petch effect. For titanium, due to the deformation twinning can refine the grain size during normal compression process, so the UAC did not reduce much grain size comparing with normal compression. As the ultrasonic vibration could promote the saturation of deformation twinning and then with less twinning boundaries in the UAC sample, the deformation twinning induced strain hardening effect was weakened, so the UAC titanium sample exhibit a residual softening effect. The ultrasonic vibration also can work similar as thermal treatment to the titanium sample and lead to the occurrence of yield point which could also contribute to the residual softening effect.

## Acknowledgements

Financial supports from the Excellence Australia, Australian Research Council (Grant no. LP130101001), Scientific Research Program of Henan University of Technology (No. 2014YWQ008), and Hong Kong Research Grants Council General Research Funds (Grant no. 11211015) are fully acknowledged. Great appreciate to Dr. Hua Chen for his help with EBSD characterization.

## References

- [1] F. Blaha, B. Langenecker, Dehnung von Zink-Kristallen unter Ultraschalleinwirkung, *Naturwissenschaften* 42 (20) (1955) 556–556.
- [2] R. Green, Non-linear effects of high-power ultrasonics in crystalline solids, *Ultrasonics* 13 (3) (1975) 117–127.
- [3] B. Langenecker, Effects of ultrasound on deformation characteristics of metals, *IEEE Trans. Sonics Ultrasonics* 13 (1) (1966) 1–8.
- [4] A. Siddiq, T. El Sayed, Acoustic softening in metals during ultrasonic assisted deformation via CP-FEM, *Mater. Lett.* 65 (2) (2011) 356–359.
- [5] H. Huang, A. Pequegnat, B. Chang, M. Mayer, D. Du, Y. Zhou, Influence of superimposed ultrasound on deformability of Cu, *J. Appl. Phys.* 106 (11) (2009) 113514.
- [6] Z. Yao, G.-Y. Kim, Z. Wang, L. Faidley, Q. Zou, D. Mei, Z. Chen, Acoustic softening and residual hardening in aluminum: modeling and experiments, *Int. J. Plast.* 39 (2012) 75–87.
- [7] B. Schinke, T. Malmberg, Dynamic tensile tests with superimposed ultrasonic oscillations for stainless steel type 321 at room temperature, *Nucl. Eng. Des.* 100 (3) (1987) 281–296.
- [8] M. Tanibayashi, A theory of the Blaha effect, *Physica Status Solidi (a)* 128 (1) (1991) 83–94.
- [9] G. Malygin, Acoustoplastic effect and the stress superposition mechanism, *Phys. Solid State* 42 (1) (2000) 72–78.
- [10] H. Kirchner, W. Kromp, F. Prinz, P. Trimmel, Plastic deformation under simultaneous cyclic and unidirectional loading at low and ultrasonic frequencies, *Mater. Sci. Eng.* 68 (2) (1985) 197–206.
- [11] O. Izumi, K. Oyama, Y. Suzuki, On the superimposing of ultrasonic vibration during compressive deformation of metals, *Trans. Jpn. Inst. Met.* 7 (3) (1966) 158–161.
- [12] A. Eaves, A. Smith, W. Waterhouse, D. Sansome, Review of the application of ultrasonic vibrations to deforming metals, *Ultrasonics* 13 (4) (1975) 162–170.
- [13] Y. Daud, M. Lucas, Z. Huang, Modelling the effects of superimposed ultrasonic vibrations on tension and compression tests of aluminium, *J. Mater. Process. Technol.* 186 (1) (2007) 179–190.
- [14] J.-C. Hung, Y.-C. Tsai, C. Hung, Frictional effect of ultrasonic-vibration on upsetting, *Ultrasonics* 46 (3) (2007) 277–284.
- [15] K. Siu, A. Ngan, I. Jones, New insight on acoustoplasticity—Ultrasonic irradiation enhances subgrain formation during deformation, *Int. J. Plast.* 27 (5) (2011) 788–800.

- [16] G.G. Harman, J. Albers, The ultrasonic welding mechanism as applied to aluminum-and gold-wire bonding in microelectronics, *IEEE Trans. Parts Hybrids Packag.* 13 (4) (1977) 406–412.
- [17] J. Tsujino, K. Hidai, A. Hasegawa, R. Kanai, H. Matsuura, K. Matsushima, T. Ueoka, Ultrasonic butt welding of aluminum, aluminum alloy and stainless steel plate specimens, *Ultrasonics* 40 (1) (2002) 371–374.
- [18] I.E. Gunduz, T. Ando, E. Shattuck, P.Y. Wong, C.C. Doumanidis, Enhanced diffusion and phase transformations during ultrasonic welding of zinc and aluminum, *Scr. Mater.* 52 (9) (2005) 939–943.
- [19] T. Kim, J. Yum, S. Hu, J. Spicer, J. Abell, Process robustness of single lap ultrasonic welding of thin, dissimilar materials, *CIRP Ann.-Manuf. Technol.* 60 (1) (2011) 17–20.
- [20] E. Mariani, E. Ghassemieh, Microstructure evolution of 6061 O Al alloy during ultrasonic consolidation: an insight from electron backscatter diffraction, *Acta Mater.* 58 (7) (2010) 2492–2503.
- [21] K. Siegert, J. Ulmer, Superimposing ultrasonic waves on the dies in tube and wire drawing, *J. Eng. Mater. Technol.* 123 (4) (2001) 517–523.
- [22] M. Murakawa, M. Jin, The utility of radially and ultrasonically vibrated dies in the wire drawing process, *J. Mater. Process. Technol.* 113 (1) (2001) 81–86.
- [23] X. Shan, H. Qi, L. Wang, T. Xie, A new model of the antifriction effect on wire drawing with ultrasound, *Int. J. Adv. Manuf. Technol.* 63 (9–12) (2012) 1047–1056.
- [24] N. Tao, M. Sui, J. Lu, K. Lua, Surface nanocrystallization of iron induced by ultrasonic shot peening, *Nanostruct. Mater.* 11 (4) (1999) 433–440.
- [25] J. Badreddine, E. Rouhaud, M. Micoulaut, D. Retraint, S. Remy, M. François, P. Viot, G. Doubre-Baboeuf, D. Le Saunier, V. Desfontaine, Simulation and experimental approach for shot velocity evaluation in ultrasonic shot peening, *Méc. Ind.* 12 (03) (2011) 223–229.
- [26] I. Lum, H. Huang, B. Chang, M. Mayer, D. Du, Y. Zhou, Effects of superimposed ultrasound on deformation of gold, *J. Appl. Phys.* 105 (2) (2009) 024905.
- [27] R. Dutta, R. Petrov, R. Delhez, M. Hermans, I. Richardson, A. Böttger, The effect of tensile deformation by in situ ultrasonic treatment on the microstructure of low-carbon steel, *Acta Mater.* 61 (5) (2013) 1592–1602.
- [28] G. Ambrogio, L. Filice, F. Gagliardi, Formability of lightweight alloys by hot incremental sheet forming, *Mater. Des.* 34 (2012) 501–508.
- [29] F. Froes, H. Friedrich, J. Kiese, D. Bergoint, Titanium in the family automobile: the cost challenge, *Jom* 56 (2) (2004) 40–44.
- [30] M. Kleiner, M. Geiger, A. Klaus, Manufacturing of lightweight components by metal forming, *CIRP Ann.-Manuf. Technol.* 52 (2) (2003) 521–542.
- [31] S. Yan, B. Xing, Q.H. Qin, Effect of Interface on the Deformation of Aluminium Bicrystal: Atomistic Simulation Study, *MATEC Web of Conferences*, EDP Sciences, 2016, pp. 02010.
- [32] T. Inoue, Z. Horita, H. Somekawa, K. Ogawa, Effect of initial grain sizes on hardness variation and strain distribution of pure aluminum severely deformed by compression tests, *Acta Mater.* 56 (20) (2008) 6291–6303.
- [33] B. Mordyuk, O. Karasevskaya, G. Prokopenko, N. Khripta, Ultrafine-grained textured surface layer on Zr–1% Nb alloy produced by ultrasonic impact peening for enhanced corrosion resistance, *Surf. Coat. Technol.* 210 (2012) 54–61.
- [34] B.N. Mordyuk, G.I. Prokopenko, Ultrasonic impact peening for the surface properties' management, *J. Sound Vib.* 308 (3) (2007) 855–866.
- [35] X. An, C. Rodopoulos, E. Statnikov, V. Vitazev, O. Korolkov, Study of the surface nanocrystallization induced by the esonix ultrasonic impact treatment on the near-surface of 2024-T351 aluminum alloy, *J. Mater. Eng. Perform.* 15 (3) (2006) 355–364.
- [36] E. Hall, The deformation and ageing of mild steel: III discussion of results, *Proceedings of the Physical Society. Section B* 64(9) (1951) 747
- [37] N. Petch, The cleavage strength of polycrystals, *J. Iron Steel Inst.* 174 (1953) 25–28.
- [38] *ASM Handbook. Vol. 2, Properties and Selection: Nonferrous Alloys and Special-Purpose Materials, tenth ed., ASM international* (1990).
- [39] R. Armstrong, I. Codd, R. Douthwaite, N. Petch, The plastic deformation of polycrystalline aggregates, *Philos. Mag.* 7 (73) (1962) 45–58.
- [40] D.A. Hughes, *Plastic Deformation Structures 2004*, ASM International, Materials Park, OH, 2004, pp. 192–206.
- [41] D. Kuhlmann-Wilsdorf, N. Hansen, Geometrically necessary, incidental and sub-grain boundaries, *Scr. Metall. Mater.* 25 (7) (1991) 1557–1562.
- [42] D.A. Hughes, N. Hansen, Microstructure and strength of nickel at large strains, *Acta Mater.* 48 (11) (2000) 2985–3004.
- [43] X. Zhang, N. Hansen, Y. Gao, X. Huang, Hall–Petch and dislocation strengthening in graded nanostructured steel, *Acta Mater.* 60 (16) (2012) 5933–5943.
- [44] N. Hansen, Hall–Petch relation and boundary strengthening, *Scr. Mater.* 51 (8) (2004) 801–806.
- [45] A. Godfrey, D. Hughes, Scaling of the spacing of deformation induced dislocation boundaries, *Acta Mater.* 48 (8) (2000) 1897–1905.
- [46] D. Chichili, K. Ramesh, K. Hemker, The high-strain-rate response of alpha-titanium: experiments, deformation mechanisms and modeling, *Acta Mater.* 46 (3) (1998) 1025–1043.
- [47] A. Panin, M. Kazachenok, A. Kozelskaya, R. Hairullin, E. Sinyakova, Mechanisms of surface roughening of commercial purity titanium during ultrasonic impact treatment, *Mater. Sci. Eng.: A* 647 (2015) 43–50.
- [48] A. Dekhtyar, B. Mordyuk, D. Savvakina, V. Bondarchuk, I. Moiseeva, N. Khripta, Enhanced fatigue behavior of powder metallurgy Ti–6Al–4V alloy by applying ultrasonic impact treatment, *Mater. Sci. Eng.: A* 641 (2015) 348–359.
- [49] S. Jelliti, C. Richard, D. Retraint, T. Roland, M. Chemkhi, C. Demangel, Effect of surface nanocrystallization on the corrosion behavior of Ti–6Al–4V titanium alloy, *Surf. Coat. Technol.* 224 (2013) 82–87.
- [50] X. Wu, S.R. Kalidindi, C. Necker, A.A. Salem, Prediction of crystallographic texture evolution and anisotropic stress–strain curves during large plastic strains in high purity  $\alpha$ -titanium using a Taylor-type crystal plasticity model, *Acta Mater.* 55 (2) (2007) 423–432.
- [51] A.A. Salem, S.R. Kalidindi, R.D. Doherty, Strain hardening regimes and microstructure evolution during large strain compression of high purity titanium, *Scr. Mater.* 46 (6) (2002) 419–423.
- [52] A. Salem, S. Kalidindi, S. Semiatin, Strain hardening due to deformation twinning in  $\alpha$ -titanium: constitutive relations and crystal-plasticity modeling, *Acta Mater.* 53 (12) (2005) 3495–3502.
- [53] A. Salem, S. Kalidindi, R. Doherty, S. Semiatin, Strain hardening due to deformation twinning in  $\alpha$ -titanium: mechanisms, *Metall. Mater. Trans. A* 37 (1) (2006) 259–268.
- [54] L. Jiang, J.J. Jonas, A.A. Luo, A.K. Sachdev, S. Godet, Twinning-induced softening in polycrystalline AM30 Mg alloy at moderate temperatures, *Scr. Mater.* 54 (5) (2006) 771–775.
- [55] Z. Li, L. Fu, B. Fu, A. Shan, Yield point elongation in fine-grained titanium, *Mater. Lett.* 96 (2013) 1–4.
- [56] M.R. Barnett, M.D. Nave, A. Ghaderi, Yield point elongation due to twinning in a magnesium alloy, *Acta Mater.* 60 (4) (2012) 1433–1443.